



SOLMED: heat transfer characterization

Armel Gonda^{a,*}, Viviane Renaudin^a, Dominique Alonso^{a,*}, Thibault Roques-Carmes^a,
Philippe Bandelier^b

^aENSIC-LRGP, UMR 7274 CNRS, 1 rue Grandville, 54001 Nancy, France, Tel. +33 383175106;

emails: armel.gonda@univ-lorraine.fr (A. Gonda), dominique.alonso@univ-lorraine.fr (D. Alonso)

^bLITEN, CEA, 17 rue des Martyrs, 38054 Grenoble, France

Received 16 April 2015; Accepted 24 December 2015

ABSTRACT

Solar multi-effect desalination (SOLMED) is a new technology based on low-temperature multi-effect distillation (LT-MED). The project aims at sea water desalination on vertical polymer tubes using thermal solar energy, or low-grade thermal waste energy. This paper presents experimental results of a test rig with a single polyolefin tube of 70 μm thick. Hydrodynamic and thermal tests were carried out in order to characterize the heat transfer. It was found that salt water flow on the outer surface of the tube improves the falling film wetting over time. Results of the overall heat transfer coefficient are presented and compared to other studies. Achieved values ranged from 1,300 to 2,600 $\text{W}/\text{m}^2 \text{K}$. Finally, two new correlations were developed from the experimental data to predict heat transfer coefficients for film evaporation outside the tube and dropwise condensation inside the tube.

Keywords: Desalination; Distillation; Low temperature; Polymer; Heat transfer; Falling film; Evaporation; Dropwise condensation

1. Introduction

Solar multi-effect desalination (SOLMED) is a new technology based on low-temperature multi-effect distillation (LT-MED) [1]. SOLMED project aims at sea water desalination on vertical polymer tubes using thermal solar energy, or low-grade thermal waste energy. A five-effect prototype was built to provide proof of concept at a significant scale [2]. Each effect consists of vertical, flexible, and thin tubes suspended from the top and free at the bottom. Sea water to be evaporated flows as a falling film on the outer surface

of tubes, while steam condenses on the inner surface. This configuration is necessary because of overpressure inside the tubes. Nominal capacity is 9.1 m^3 per day for a heat consumption of 60 kW [1,2]. Each effect comprises 19 polymer tubes to develop a total area of 7.4 m for heat transfer.

Aluminum and cupronickel are commonly used as heat transfer surfaces in conventional MED systems. These materials are expensive, and they are affected by sea water corrosion. Indeed, an annual corrosion allowance of about 25–50 μm must be made for these materials [3]. Due to the high corrosivity of sea water, corrosion resistant polymers can be a reasonable alter-

*Corresponding authors.

Presented at EuroMed 2015: Desalination for Clean Water and Energy, Palermo, Italy, 10–14 May 2015.
Organized by the European Desalination Society.

native to metals for LT-MED [4]. Scheffler and Leao [5] noted that polyolefins such as high-density polyethylene (HDPE) and polypropylene (PP) have better resistance than these metals, which permits thinner walls. Furthermore, untreated polyolefins surfaces resist the adhesion of scale by anti-stick property. If scale formation occurs, surface flexibility breaks the deposit from the wall. Under these corrosive, scaling, and fouling conditions, thin polymers walls have excellent behavior. Finally, the use of such surfaces reduces cost and environmental impact by lowering the amount of chemicals needed for pretreatment [1]. However, thermal conductivity of polymers is quite low: 0.1–0.5 W/m K [6]. It is almost 100 times less than common metals. For this reason, it is necessary to use very thin walls.

Recently, Christmann et al. [4,6,7] carried out mechanical and thermal studies on a polyetheretherketone (PEEK) plate of 25 μm thick. In SOLMED process, heat transfer surfaces are polyolefin tubes of 50–70 μm thick. A single-tube test rig was built and experimental tests were carried out to characterize heat transfer through these tubes. Then, experimental results were used to develop a new predictive model. The final aim is to enrich the thermal and hydraulic model used in SOLMED simulation tool. Currently, this tool describes the heat transfer only in terms of overall heat transfer coefficient (U). U depends on sea water film evaporation outside the tube, wall thermal resistance, and dropwise condensation inside the tube. To reach each contribution, thermal conductivity is measured, and appropriated heat transfer coefficient correlations are considered.

There are many correlations for non-boiling film evaporation in the literature. Some of them are summarized in Table 1 (from [8]). Different dimensionless numbers are used in this table.

The falling film evaporation Nusselt number (Nu) is usually defined as follows:

$$Nu = \frac{h_{\text{evap}}}{k} \cdot \left(\frac{v^2}{g}\right)^{1/3} \quad (1)$$

where h_{evap} is the filmwise evaporation heat transfer coefficient ($\text{W}/\text{m}^2 \text{K}$), k is the liquid thermal conductivity ($\text{W}/\text{m K}$), v is the liquid kinematics viscosity (m^2/s), and g is the gravitational acceleration (m/s^2).

The falling film Reynolds number is expressed as follows:

$$Re = \frac{4 \cdot \Gamma}{\mu} \quad (2)$$

where Γ is the mass flow-rate per unit tube perimeter ($\text{kg}/\text{s m}$) and μ is the liquid dynamic viscosity (Pa s).

The Prandtl number is expressed as follows:

$$Pr = \frac{\mu \cdot Cp}{k} \quad (3)$$

where Cp is the liquid heat capacity ($\text{J}/\text{kg K}$).

Finally, the Kapitza number is expressed as follows:

$$Ka = \frac{g \cdot \mu^4}{\rho \cdot \sigma^3} \quad (4)$$

where ρ is the liquid density (kg/m^3) and σ is the liquid/vapor surface tension (N/m).

In Table 1, Chun and Seban [10] correlation was developed with a similar geometry to that used in this study (i.e. outside of vertical tube). Therefore, this correlation is used thereafter to develop a new correlation for film evaporation from experimental results.

Unlike film evaporation, there are very few correlations for dropwise condensation reported in the literature. Bonner [13] developed two of them, a non-heat flux dependant (Eq. (5)) and a heat flux dependant (Eq. (6)). They accurately model experimental data previously acquired for several fluids at different temperatures. When water is used, heat flux dependant correlation (Eq. (6)) is recommended:

$$h_{\text{cond}} = 33 \cdot \frac{k}{r_d^{2/3} \cdot r_i^{1/3}} \cdot \left(\frac{\sin \theta}{1 - \cos \theta}\right) \quad (5)$$

$$h_{\text{cond}} = 2.7 \cdot \frac{k}{r_d^{1/2} \cdot r_i^{1/4} \cdot r_t^{1/4}} \cdot \left(\frac{\sin \theta}{1 - \cos \theta}\right) \quad (6)$$

where h_{cond} is the dropwise condensation heat transfer coefficient ($\text{W}/\text{m}^2 \text{K}$), θ is the contact angle ($^\circ$), r_d is the departing droplet radius (m), r_i is the effective length (m), and r_t is the minimum droplet radius (m). Developed by Bonner [13], the last three parameters are defined as follows:

$$r_d = \left(\frac{\sigma}{\rho \cdot g}\right)^{1/2} \quad (7)$$

$$r_i = \frac{k \cdot T_{\text{cond}}}{\rho_v \cdot Lv^2} \cdot \left(\frac{\sin \theta}{1 - \cos \theta}\right) \cdot \left(\frac{\gamma + 1}{\gamma - 1}\right) \cdot \left(\frac{R_g \cdot T_{\text{cond}}}{2\pi}\right)^{1/2} \quad (8)$$

Table 1
Experimental correlations for non-boiling evaporation of falling water film [8]

Authors	Material and geometry	Heating method	Pr range	Re range	Correlations for film side heat transfer
Kafi et al. [9]	Stainless steel plate with metallic grids to promote film turbulences; Height: 1.8 m; width: 0.4 m	Hot water	3.5	100–800	$Nu_{tur} = 0.0033 \cdot Re^{0.4} \cdot Pr^{0.65}$
Chun and Seban [10]	Outside of vertical stainless steel tube; Diameter: 0.029 m; heated length: 0.292 m	Electrical	1.77–5.7	320–21 000	$Nu_{lam} = 0.821 \cdot Re^{-0.22}$ $Nu_{tur} = 0.0038 \cdot Re^{0.4} \cdot Pr^{0.65}$ Transition: $Re = 5900/Pr^{1.06}$
Alhousseini et al. [11]	Outside of vertical stainless steel tube; Diameter: 0.0381 m; length: 2.9 m	Electrical	1.73–46.6	34–15 600	$Nu = (Nu_{lam}^5 + Nu_{tur}^5)^{1/5}$ $Nu_{lam} = 2.65 \cdot Re^{-0.158} \cdot Ka^{0.0563}$ $Nu_{tur} = \frac{Pr \cdot \delta^{+1/3}}{(A_1 \cdot Pr^{3/4} + A_2 \cdot Pr^{1/2} + A_3 \cdot Pr^{1/4} + C_1) + (B \cdot Ka^{1/2} \cdot Pr^{1/2})}$ where $A_1 = 9.17$ $A_2 = 0.328 \cdot \pi \cdot (130 + \delta^+) / \delta^+$ $A_3 = 0.0289 \cdot (152100 + 2,340 \delta^+ + 7 \cdot \delta^{2+}) / \delta^{2+}$ $B = 2.51 \cdot 10^6 \cdot \delta^{+0.333} \cdot Ka^{-0.173} / Re^{(3.49Ka^{0.0675})}$ $C_1 = 8.82 + 0.0003 \cdot Re$ $\delta^+ = 0.0946 \cdot Re^{0.8}$
Han and Fletcher [12]	Horizontal brass tube: smooth, circumferentially and axially grooved. Diameter: 0.0508 m; length: 0.254 m	Electrical	1.3–3.6	770–7,000	$Nu_{tur} = 0.025 \cdot Re^{0.2} \cdot Pr^{0.53}$ (smooth-tube) $Nu_{tur} = 0.0028 \cdot Re^{0.5} \cdot Pr^{0.85}$ (grooved-tube)

$$r_t = \frac{2 \cdot \sigma \cdot T_{cond}}{\rho \cdot Lv \cdot \Delta T_{cond}} \quad (9)$$

where T_{cond} is the condensation temperature (K), ρ_v is the vapor density (kg/m^3), Lv is the latent vaporization heat (J/kg), γ is the heat capacity ratio (–), R_g is the specific ideal gas constant (J/kg K), and ΔT_{cond} is the condensation/wall temperature difference (K).

Following the Bonner's [13] recommendation, Eq. (6) is used thereafter to develop a new correlation for dropwise condensation from experimental results.

Results of heat transfer characterization through the tube are presented in the following sections of this paper. The test rig and the experimental conditions are first exposed in detail, then hydrodynamic aspects are investigated. Afterward, thermal test results are

discussed and compared with literature. Finally, new correlations for film evaporation and drop condensation, based on our experimental results, are proposed in order to enrich the global model used in SOLMED simulation tool.

2. Experiment

2.1. Experimental apparatus

A single-tube test rig has been built to characterize heat transfer in SOLMED operating conditions. Fig. 1 shows a simplified schematic (a) and two pictures (b) of the experimental setup. The whole installation footprint is 2×4 m, with a height of about 3 m. The use of heat PVC tubes (see Fig. 1(b)) limits maximum operating temperature at 80°C , which corresponds to

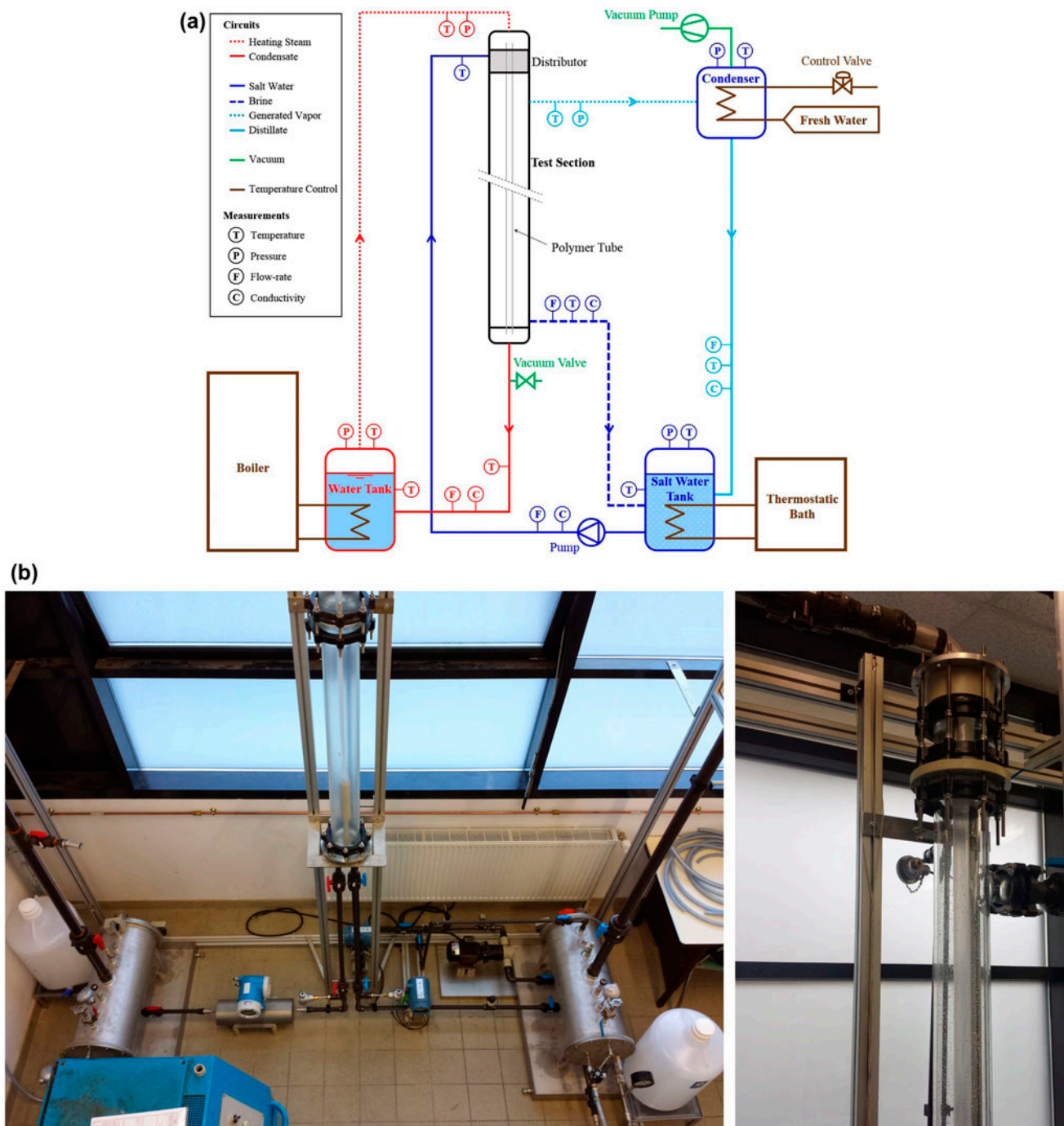


Fig. 1. Experimental setup schematic (a) and pictures (b).

an absolute pressure of about 500 mbar. Thus, the process is performed under reduced pressure. It was designed to operate over the range of 25–70°C (i.e. 32–312 mbar abs.). This range covers the operating conditions of SOLMED prototype [2] (40–65°C, i.e. 74–250 mbar abs.). The setup comprises temperature-controlling devices (brown in Fig. 1(a)), the test

section, a condenser, two water tanks, and associated instruments for temperature, pressure, flow-rates, and conductivity measurements. Electrical control circuits, isolation valves, safety devices, additional sensors, and pressure-control circuits are not shown. There are two main circuits: heating circuit (red lines) and salt water circuit (blue lines).

In the heating circuit, saturated steam (dotted red line in Fig. 1(a)) is produced from distilled water in the tank. It flows to the test section where it condenses inside the polymer tube. Condensed water (red line) is collected at the bottom of test section and then returns to the water tank for recycling. The temperature in the water tank, and consequently the steam temperature and pressure inside the tube, are controlled by the oil boiler (SISE Parmilleux, XH20r13, 22 kW). The valve below test section allows evacuation of accumulated non-condensable gases inside the tube.

In the salt water circuit, sodium chloride solution (NaCl), with a concentration of 35 g/l, is pumped from the tank to the distributor (dark blue line in Fig. 1(a)) by a magnetic drive sliding rotary vane pump (AB Pompes, VPA 04 PP). Salt water enters the distributor with a temperature very close to the boiling temperature in order to reduce salt water film pre-heating. Salt water temperature can be slightly subcooled, but never overheated to avoid flash. In the distributor, the solution is uniformly spread on the tube outer surface and then flows down by gravity by forming a thin liquid film. Heated by condensing steam inside the tube, the salt water film is partially evaporated. Nucleate boiling was never observed because of low temperature differences. Therefore, all the evaporation takes place from the surface of the film as previously reported by Chun and Seban [10]. While vapor flows against liquid film flow toward the condenser (light blue dotted line), the residual brine is collected at the bottom of the test section and returns (dark blue dotted line) to the salt water tank. Liquid temperature in this tank is controlled by a thermostatic bath (Huber, HS40, 0.6 kW at -10°C). Meanwhile, distillate produced at condenser is collected and also returns (light blue line) to the tank. As for tube inside, non-condensable gases in the condenser can be evacuated by a diaphragm vacuum pump (Vacuubrand, MD4 NT Vario). Evaporation side temperature in the test section (i.e. pressure also) is controlled by the condenser. For that purpose, the cooling water circuit supplying the condenser has a manual control valve. The latter, has a very important role in setting operating conditions.

2.2. Test section

The test section is the main component of the system. As can be seen in Fig. 1(b), it includes the polymer tube in a glass column of 100 mm in diameter and a total height of 2 m. The outer glass column was not insulated in order to observe the salt water wetting on the tube. At room temperature, tube effective

length is about 1.75 m. It has a diameter of 32 mm and a thickness of 70 μm , which corresponds to a surface area of 0.176 m^2 . Tube fabrication and characterization are discussed in [1]. The tube is held by two fixing parts, an upper and a lower. The upper one is the distributor, it ensures physical separation between heating steam and salt water feed. Its most important function is to spread salt water on tube periphery in form of thin, continuous, and uniform film. By its weight, the lower fixing part ensures tube vertical tension. It also separates the heating and salt water circuits, so leakage due to pressure difference is avoided. At the same time, its design allows free thermal expansion of the tube.

2.3. Experimental procedure and uncertainty analysis

Measurements were performed for five evaporation temperatures ($T_{\text{evap}} = 25, 30, 40, 50, \text{ and } 65^{\circ}\text{C}$) with a film Reynolds number varying from 910 to 4,220. Table 2 gives the range of parameters covered experimentally.

Before tests, the diaphragm pump was used to adjust vacuum conditions of the setup. Leakages were checked by a helium leak detector (Adixen ASM 142) and coated with mastic (Diatex LSM1310). This helped to make the experimental setup airtight under vacuum conditions for several days. The pressure increased by about 0.5 mbar per day. Distilled water and salt water were charged by siphon into each tank, and were degassed by boiling. Then, non-condensable gases were removed by the vacuum pump.

For tests performed at the highest evaporation temperatures (T_{evap}), 12 h equilibration time is needed to reach steady state. And, for a fixed-temperature difference (ΔT), it takes 24 h to obtain steady state before performing tests with varying salt water flow-rate (F_{swt}).

A total of 415 experimental runs were carried out to investigate the heat transfer through the tube. Each measured variable used in the calculations is the result of the arithmetic average of approximately 200 data readings. To reduce errors, each measurement was repeated three times under the same experimental conditions. Therefore, each experimental point in Fig. 7 was obtained by averaging these three measurements.

Then the heat transfer coefficients were calculated from temperature and flow-rate measurements. Platinum resistance sensors (Pt100, TC Direct, $0\text{--}200^{\circ}\text{C}$) were used to measure temperatures. Saturation temperatures were also deduced from pressure measurements with absolute pressure sensors (Keller PAA33X,

Table 2
Experimental conditions

Evaporation side	Approximate saturation temperature, T_{evap} (°C)		25	30	40	50	65
	Approximate absolute pressure, P_{evap} (mbar)		32	42.5	74	123.5	250
	Approximate Prandtl number, Pr		6.3	5.59	4.51	3.73	2.91
Salt water feed	Inlet falling film flow-rate, F_{swf} (l/h)	Minimum	85.1	68.4	72	71.8	65.9
		Maximum	178.4	178	177.8	176.1	177.9
	Inlet falling film Reynolds number, Re_{swf}	Minimum	1,010	910	1,150	1,370	1,560
		Maximum	2,120	2,360	2,850	3,350	4,220
Condensation side	Saturation temperature, T_{cond} (°C)	Minimum	25.9	31.3	41	51	66.9
		Maximum	35.1	38	46	55.3	70.2
	Absolute pressure, P_{cond} (mbar)	Minimum	34	44	76.5	129	273
Maximum		55	65	100	159	315	
Across tube	Temperature difference, ΔT (K)	Minimum	1.1	1	1	1.1	2
		Maximum	3.2	6.1	6	5.1	5.1
	Pressure difference, ΔP (mbar)	Minimum	2	2	3	6	23
		Maximum	22	21	26	35	65

0–500 mbar). Electromagnetic flow meters (Rosemount 8711, 0–200 l/h) were used to measure salt water and brine flow-rates. Associated with a LabVIEW computer interface, a data acquisition system (National Instruments) was used for real-time monitoring and control of the installation.

Table 3 shows measurement accuracy. Distillate and condensate flow-rates were measured by potting with transparent Altuglas® volumetric tubes ($D_i = 0.014$ m and $H = 0.45$ m). Measurement accuracy for these flow-rates was calculated with an uncertainty of ± 0.1 mm on the diameter, ± 4 mm on the height, and 0.5 s on time. The latter reasonably represents operator’s reaction and chronometer uncertainties. It should be noted that the uncertainties on tube diameter and length were also estimated. Finally, conductivity measurements were performed to check for short circuiting between the two water circuits.

Error propagation analysis was performed with Engineering Equation Solver (EES) software according to Taylor and Kuyatt [14] study. Thermophysical properties of water (Steam_IAPWS [15,16]) and salt water

(SW_Property [17]) were also calculated with this software. Thus, errors on fluids properties have also been taken into account. Error bars for some calculated overall heat transfer coefficients are displayed in Fig. 8.

2.4. Data interpretation

For calculations, the following assumptions were made:

- (1) Saturated heating steam is assumed and it condenses inside tube at saturation temperature, T_{cond} .
- (2) All condensation heat is transferred through the tube for evaporation of the salt water film.
- (3) The salt water film is spread on the tube at saturation temperature, which corresponds to brine temperature. The temperature remains constant along the tube.
- (4) All the evaporation takes place from the salt water film surface at water saturation temperature, T_{evap} .
- (5) Thermophysical properties of salt water film are evaluated at saturation temperature and do not change over the whole tube length because only a small fraction of the flow is evaporated.
- (6) Pressure drop on both sides are neglected.
- (7) Scaling and fouling are neglected.
- (8) Shear forces between gas and liquids are neglected.

Fig. 2 shows a schematic view of heat transfer through the tube. As the temperature outside the glass column is always less than the temperature inside, the generated vapor is partially condensed on the inner

Table 3
Measurement accuracy

Items	Accuracy
Temperature	± 0.1 °C
Pressure	± 0.5 mbar
Salt water and brine flow-rates	± 2 l/h
Condensate and distillate flow-rates	± 0.02 g/s ^a
Tube diameter	± 0.2 mm ^a
Tube length	± 2 mm ^a

^acalculated values.

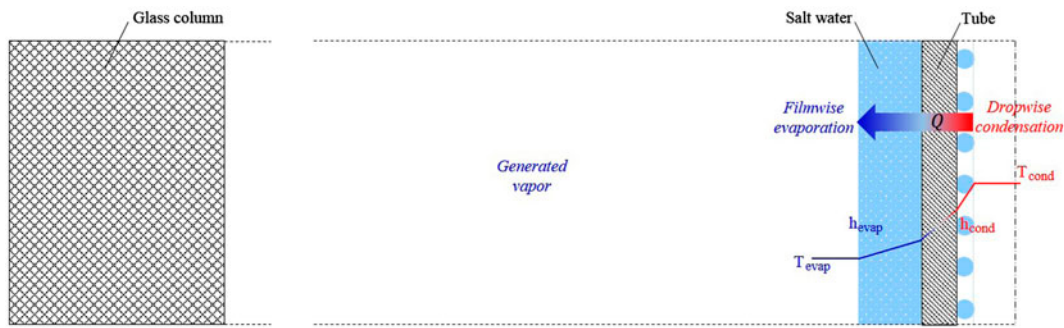


Fig. 2. Schematic view of heat transfer through the tube.

surface of the glass tube. That's why the heat balance was conducted from the condensate within the polymer tube. The overall heat flux released inside the tube, transferred through tube wall and received by the evaporating salt water film is calculated as follows:

$$Q = \dot{m}_{\text{cond}} \cdot Lv \quad (10)$$

where Q is the overall heat flux (W) and \dot{m}_{cond} is the condensate flow-rate (kg/s).

The overall heat transfer coefficient can be calculated according to:

$$U = \frac{Q}{A_e \cdot \Delta T} \quad (11)$$

where U is the overall heat transfer coefficient ($\text{W}/\text{m}^2 \text{K}$), A_e is the outer heat transfer area (m), and $\Delta T = T_{\text{cond}} - T_{\text{evap}}$ is the overall temperature difference (K).

U is related to evaporation and condensation heat transfer coefficients by the basic equation for cylindrical tube [18]:

$$\frac{1}{U} = \frac{1}{h_{\text{evap}}} + \frac{A_e \cdot \ln(A_e/A_i)}{2\pi \cdot L \cdot \lambda} + \frac{A_e}{h_{\text{cond}} \cdot A_i} \quad (12)$$

where A_i is the inner heat transfer area (m), L is the tube length (m), and λ is the wall thermal conductivity ($\text{W}/\text{m K}$).

3. Results and discussion

3.1. Hydrodynamic results

Hydrodynamic tests were performed to study salt water film wetting on the tube surface. As said before, the aim of the distribution system is to spread salt water on tube periphery in form of thin, continuous, and uniform film. For this reason, attention was given to the design of the water distribution system in order to avoid maldistribution at the top of the tube.

Beside a proper design of the distributor, film stability is the other parameter that highly influences wetting. Indeed, stability of liquid films on a non-wettable surface is a serious issue. Surface tension effects tend to maintain dry zones in the falling film [19], as a result, the film flows in form of rivulets (see Fig. 3(a)) or it breaks forming an arch (Figs. 3(b) and (c)). These phenomena appear for low flow-rates and/or high heat flux. Above critical flow-rate any dry zones would be swept away. When the increasing flow-rate reaches this critical value, gravity and inertia effects predominate over surface tension effect, so that all dry zones will be covered by the film [20].

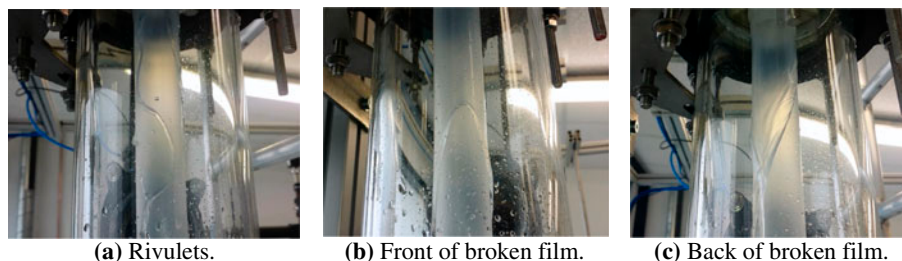


Fig. 3. Salt water film instabilities: (a) rivulets, (b) front of broken film and (c) back of broken film.

When the flow-rate varies, it has been shown that decreasing flow-rate provides better surface area wetting compared to increasing one, even at low flow-rates [8,19,21]. This is the wetting hysteresis phenomenon. Therefore, tests were carried out by decreasing salt water film flow-rate. However, maximum flow-rates (see Table 2) were limited by distributor liquid load height. Consequently, critical flow-rates were not reached during experiments, and thus dry zones remained. Yet, when salt water flows at these maximum flow-rates for a sufficiently long time, a gradual wet surface area increase has been observed. In fact, the ark of film progressively down along the tube. Therefore, the first time it takes about three hours to fully wet a new tube, whereas for the following tests on the same tube, salt water film is established within only few minutes. To understand the phenomenon, salt water contact angle measurements were carried out on a new tube (see Fig. 4(a)), and after six months of tests, on the used tube (see Fig. 4(b)). The 2 values given in Fig. 4 are each one the average of 10 contact angle measurements. The standard deviations (SD) are also given. These measurements were performed at room temperature and in equilibrium with ambient air using OCA 15 EC type measuring instrument from Dataphysics.

These measurements clearly emphasize that the new tube has a hydrophobic surface ($\theta > 90^\circ$), which is not the case for the used tube. This results in a decrease of the contact angle value of approximately 22%. This confirms the previous observation of wetting improvement over time. The modification of the tube surface properties is probably due to a very slight scaling or fouling (not visible) [2]. It would precipitate gradually while salt water is flowing as rivulets and broken film. According to this phenomenon, tube surface area has been entirely wetted at maximum flow-rates. Then, the flow-rates was decreased to minimum values (see Table 2) without dewetting the tube because of the wetting hysteresis phenomenon [8,21]. It is important to mention that the minimum flow-rates were not adjusted due to the dry zones

formation on tube surface, but rather than due to dewatering of the distributor channels.

These hydrodynamic results are essential since a good wetting of the tube surface area is necessary to ensure an efficient evaporation, especially for low flow-rates.

3.2. Thermal results

According to the findings of the hydrodynamic study, all the thermal tests were carried out with a decreasing flow-rate after waiting for complete wetting of the tube surface area.

3.2.1. Drop condensation

Two condensation modes may occur on the surface of a material: film condensation and drop condensation. Heat transfer coefficients for drop condensation are much higher than for film condensation. In this study, drop condensation was initially assumed because of tube hydrophobicity [22]. Besides the experiment, a theoretical study was conducted in order to determine the condensation mode.

Contact angle method was used to predict the condensation mode (Table 4). However, contact angles were measured at room temperature and in equilibrium with ambient air, but did not prove useful for determining the wettability of systems where mass transfer takes place [23]. To know which condensation mode prevails, Ma et al. [24,25] put forward a surface free energy criterion, i.e. the surface free energy difference between the condensate liquid at the condensation temperature and the solid surface (Table 4 and Eqs. (13)–(16)), to predict whether film condensation or drop condensation mode will prevail. Free energy criterion is not affected by the measuring temperature of the contact angles. Consequently, it is more convenient and accurate to use this method, rather than the contact angle, to predict the condensation mode.

The surface free energy difference is defined as follows:

$$\Delta\sigma = \sigma_l - \sigma_s \quad (13)$$

where σ_l and σ_s are the surface free energies of liquid and solid, respectively (N/m). The surface free energy of a solid (σ_s) depends only on its composition and chemical structure, and can be calculated from measured contact angles at room temperature for low-surface free energy solids such as polymers. Owens' [26] correlations can be used:

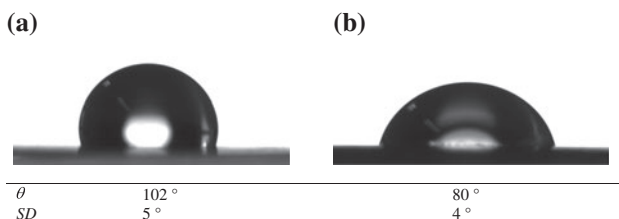


Fig. 4. Salt water drop morphologies on the outer surface of the new and used tube: (a) new tube and (b) used tube.

Table 4
Condensation mode criteria [24]

Surface free energy difference method	Contact angle method	Condensation mode
$\Delta\sigma \leq 0$	–	Film
$0 \leq \Delta\sigma < 0.0333$	$0^\circ \leq \theta < 90^\circ$	Mixed
$\Delta\sigma \geq 0.0333$	$\theta \geq 90^\circ$	Drop

$$\sigma_s^p = \left(\frac{137.5 + 256.1 \cdot \cos \theta_{\text{H}_2\text{O}} - 118.6 \cdot \cos \theta_{\text{CH}_2\text{I}_2}}{44.92} \right)^2 \times 10^{-3} \quad (14)$$

$$\sigma_s^d = \left(\frac{139.9 + 181.4 \cdot \cos \theta_{\text{CH}_2\text{I}_2} - 41.5 \cdot \cos \theta_{\text{H}_2\text{O}}}{44.92} \right)^2 \times 10^{-3} \quad (15)$$

$$\sigma_s = \sigma_s^p + \sigma_s^d \quad (16)$$

where σ_s^p and σ_s^d are the polar and dispersion component of the surface energy, respectively (N/m).

Following the same procedure as for salt water, pure water ($\theta_{\text{H}_2\text{O}}$), and diiodomethane ($\theta_{\text{CH}_2\text{I}_2}$) contact angles were measured on the inner surface of a new tube (Fig. 5). Water contact angle measurements on the used tube gave the same value as in Fig. 5(a).

Calculation results for Eqs. (13)–(16) give: $\sigma_s^p = 80.29 \times 10^{-6}$ N/m, $\sigma_s^d = 37.78 \times 10^{-3}$ N/m, $\sigma_s = 37.86 \times 10^{-3}$ N/m, and $0.0266 \leq \Delta\sigma \leq 0.034$ N/m. Therefore, it can be concluded that the condensation mode on the tube is mixed or drop condensation. It may be noted that results are rather at the high end of the mixed condensation range (Table 4). Furthermore, the contact angle method predicts a strictly drop condensation mode. So, we can conclude that drop condensation prevails inside the tube. And as said before, it remains over time. These findings are consistent with our experimental observations. Fig. 6 shows three successive images extracted from a video of drop condensation on the inner surface of the tube. This means

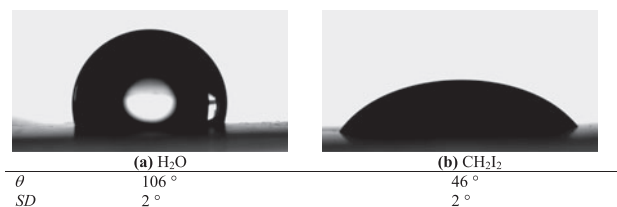


Fig. 5. Water and diiodomethane drop morphologies on the inner surface of the tube: (a) H₂O and (b) CH₂I₂.

that between the camera and drops, there are the glass column wall, the steam generated by evaporation, the falling salt water film, and finally the tube wall.

As can be seen in Fig. 6, drops appear everywhere on the inner tube surface. They grow by condensation on their surface and by coalescence. On the three images, there is a large drop which falls very quickly. It grows by collecting other drops in its path. So, inner tube surface is swept by such numerous moving drops. Therefore, lower part of the tube is swept more frequently than the upper. Consequently, only drops near the top can reach the size at which gravity exceeds the net surface tension restraining force [22].

3.2.2. Experimental overall heat transfer coefficient

To determine the experimental overall heat transfer coefficient (U_{exp}), heat flux was calculated according to Eq. (10). Then, U_{exp} was estimated with Eq. (11). Experimental results are shown in Figs. 7 and 8.

Fig. 7 plots the overall heat transfer coefficient (U_{exp}) as a function of salt water film Reynolds number (Re_{swf}) for different evaporation temperatures (T_{evap}). For comparison, the results of Christmann et al. [4] and Kafi et al. [27,28] are also plotted in Fig. 7.

Christmann et al. [4] used a 25- μm thick PEEK plate evapo-condenser with a spacer grid. They worked at three falling film inlet temperature (54.1, 54.6, and 57°C) for three heating temperatures, respectively (59, 59.1, and 60.9°C). Their overall heat transfer coefficient values range from about 3,200 to 3,800 W/m² K.

Kafi et al. [27,28] used a metallic plate evapo-condenser with a spacer grid. These results were obtained in the second stage of their pilot plant, i.e. for evaporation temperatures between 55 and 63°C, and for temperature differences between 3 and 5°C. Their overall heat transfer coefficient values range between 2,100 and 3,700 W/m² K.

The overall heat transfer coefficient (U_{exp}) as a function of temperature difference (ΔT) for two different evaporation temperatures (T_{evap}) and at fixed salt water film Reynolds numbers (Re_{swf}) is shown in



Fig. 6. Drop condensation on the inner surface of the tube.

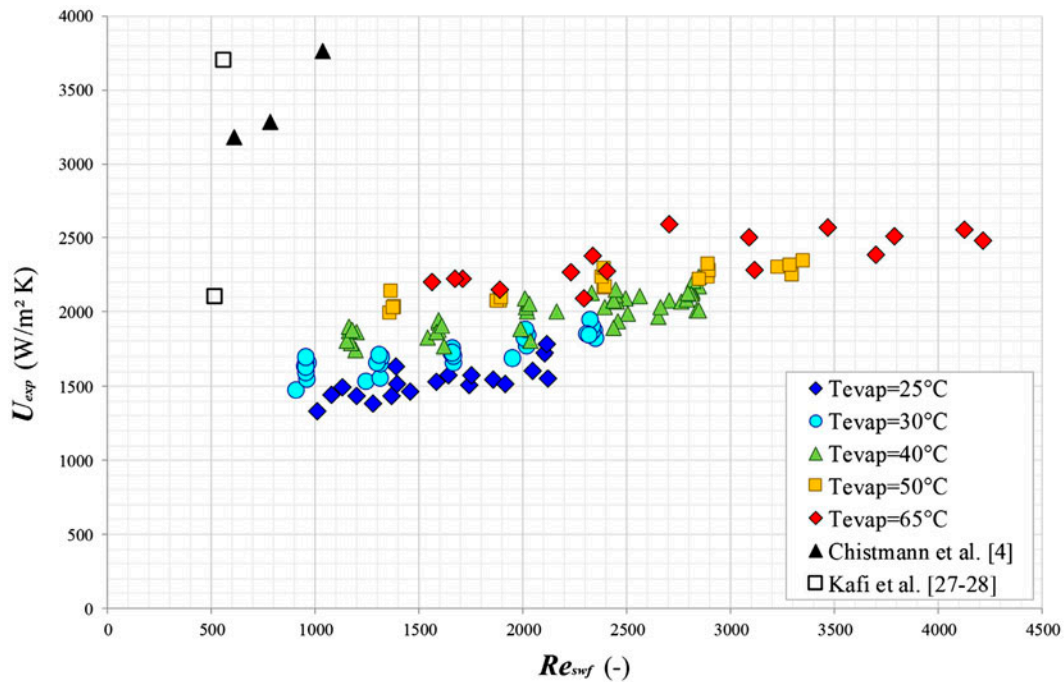


Fig. 7. Overall heat transfer coefficient vs. salt water film Reynolds number.

Fig. 8. This figure also displays error bars on the overall heat transfer coefficient values.

As shown in Fig. 7, the experimentally obtained overall heat transfer coefficient increases with the salt water film Reynolds number. This implies that the flow regime of the falling salt water film is turbulent. There is also a parametric effect due to the temperature level: for the same salt water film Reynolds number, U_{exp} increases with T_{evap} . From Fig. 8, it can be seen that overall heat transfer coefficient increases with the temperature difference. An interpretation of this behavior can be given using the heat transfer model presented hereafter in the text. Since the experi-

mental results are obtained maintaining the evaporation temperature (T_{evap}) constant, when ΔT increases, the condensation temperature (T_{cond}) does the same. Hence, ΔT influences the condensation heat transfer coefficient (h_{cond}) mainly through the minimum droplet radius (r_t) term at the denominator of Eq. (6). According to Eq. (9), r_t decreases with T_{cond} . Finally, the increase in h_{cond} with ΔT leads to an increase in the overall heat transfer coefficient (U_{exp}).

The experimental values of the overall heat transfer coefficient range from about 1,300 to 2,600 W/m² K. These values correspond to those expected. By comparing with Christmann et al. [4]

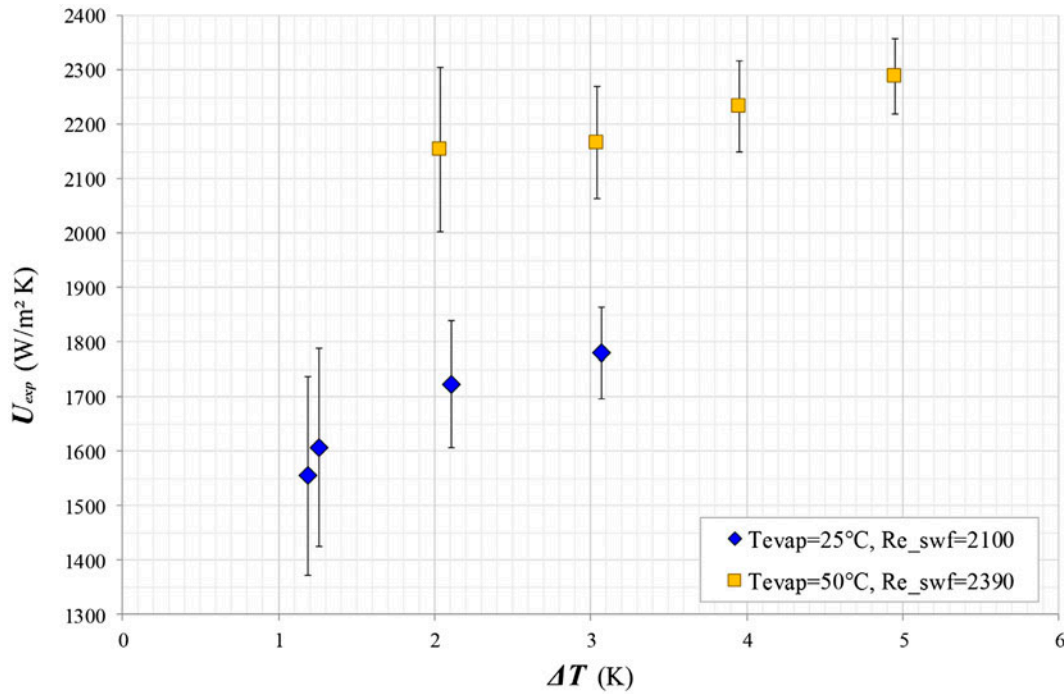


Fig. 8. Overall heat transfer coefficient vs. temperature difference.

and Kafi et al. [27] studies, our results are lower. Moreover, these authors obtained results for Reynolds number smaller than ours ($Re \leq 1000$).

This is unsurprising since those results were obtained with different geometries (i.e. plate evaporator) and different distribution systems. Furthermore, these authors used spacer grids on the evaporation side, which tends to enhance heat transfer rate acting as turbulence promoters [4,6,9,29–31]. Although Christmann et al. [4] used a polymer heat transfer surface, their results are comparable to those from Kafi et al. [27], who used metallic surface. Indeed, in MED systems it is more interesting to have large thermal performances with low salt water film Reynolds number and temperature difference as low as possible.

3.2.3. Heat transfer modeling

Based on the experimental results presented in Fig. 7, new correlations for film evaporation and drop condensation are proposed. They were developed from Chun and Seban [10] correlation for turbulent flow (see Table 1), and from Bonner's [13] heat flux-dependant correlation (see Eq. (6)):

$$Nu = \frac{h_{\text{evap}}}{k} \cdot \left(\frac{v^2}{g}\right)^{1/3} = a \cdot Re^x \cdot Pr^y \quad (17)$$

$$h_{\text{cond}} = b \cdot \frac{k}{r_d^{1/2} \cdot r_i^{1/4} \cdot r_t^{1/4}} \cdot \left(\frac{\sin \theta}{1 - \cos \theta}\right) \quad (18)$$

Inner and outer wall temperatures, $T_{w,i}$ and $T_{w,e}$, respectively, in ($^{\circ}\text{C}$), were calculated from the two following equations:

$$T_{w,e} = \frac{Q}{h_{\text{evap}} \cdot A_e} + T_{\text{evap}} \quad (19)$$

$$T_{w,i} = \frac{Q \cdot \ln(A_e/A_i)}{2\pi \cdot L \cdot \lambda} + T_{w,e} \quad (20)$$

According to the least square method, a numerical optimization was used to determine the parameters in Eqs. (17) and (18): a , x , y , and b . These four parameters were initialized with values from the original correlations. generalized reduced gradient (GRG) resolution method was used, and the solver converged to this solution:

$$a = 0.0237, x = 0.17, y = 0.32 \text{ and } b = 1.54.$$

Eqs. (21) and (22) give the final two correlations developed from our experimental results in order to predict heat transfer coefficients for film evaporation outside the tube and drop condensation inside the tube:

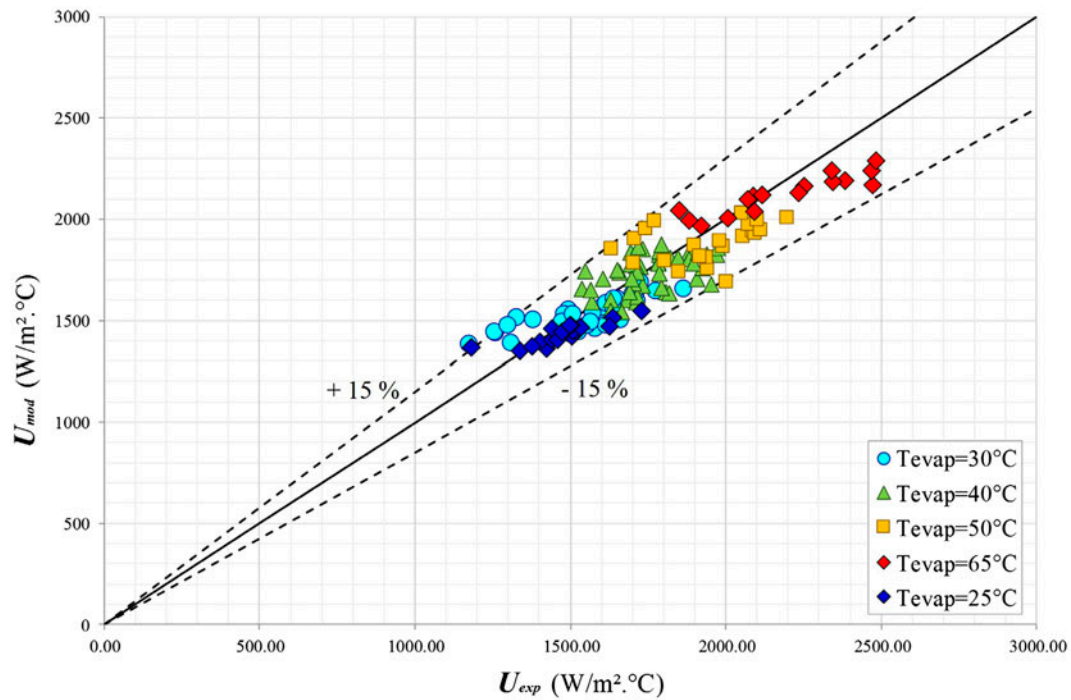


Fig. 9. Comparison between the model and the experimental results.

$$h_{\text{evap}} = 0.0237 \cdot Re^{0.17} \cdot Pr^{0.32} \cdot \left(\frac{v^2}{g \cdot k^3} \right)^{-1/3} \quad (21)$$

$$h_{\text{cond}} = 1.54 \cdot \frac{k}{r_d^{1/2} \cdot r_i^{1/4} \cdot r_t^{1/4}} \cdot \left(\frac{\sin \theta}{1 - \cos \theta} \right) \quad (22)$$

Coupling these two previous correlations to Eq. (12), it is possible to calculate the prediction for the overall heat transfer coefficient (U_{mod}). As shown in Fig. 9, good agreement has been observed between our experimental data and the model with an error of $\pm 15\%$.

4. Conclusion

Based on the operating principle of solar multi-effect desalination (SOLMED) system, a test rig with a single-polyolefin tube of 70 μm thick was built and tests were carried out to characterize heat transfer through the tube.

A hydrodynamics study has shown that the salt water flow on the outer surface of the tube improves the film wetting over time. This results in a decrease of the contact angle value of approximately 22%. According to this phenomenon, the tube surface area has been entirely wetted.

A comprehensive study on the condensation mode has demonstrated that drop condensation occurs inside the tube and remains over time. After that, overall heat transfer coefficients were evaluated and compared with literature. The experimental values ranged from 1,300 to 2,600 $\text{W}/\text{m}^2 \text{K}$. The results correspond to expected values. Although lower, the results of this study are comparable to literature data, when considering that a 25- μm -thick polymer plate heat transfer surface was used, resulting in heat transfer coefficients of 3,200–3,800 $\text{W}/\text{m}^2 \text{K}$.

Finally, two new correlations were developed from our experimental data to predict salt water film evaporation outside the tube and water drop condensation inside the tube. Good agreement has been observed between experimental data and theoretical prediction with an error of $\pm 15\%$. These theoretical models will be validated and adjusted with the prototype results, and then they will be included in SOLMED simulation tool.

Acknowledgments

SOLMED is funded by the French National Research Agency under project reference ANR-11-SEED-002. It benefits from the support of the energy clusters Tenerrdis and Capenergies.

Symbols

a	— constant in Eq. (17) (–)
A	— tube heat transfer surface area (m ²)
A_1	— parameter defined in Table 1
A_2	— parameter defined in Table 1
A_3	— parameter defined in Table 1
b	— constant in Eq. (18) (–)
B	— parameter defined in Table 1
C_1	— parameter defined in Table 1
C_p	— liquid heat capacity (J/kg °C)
D	— diameter (m)
F	— volumetric flow-rate (l/h)
g	— gravitational acceleration (m/s ²)
h	— heat transfer coefficient (W/m ² K)
H	— height (m)
k	— liquid thermal conductivity (W/m K)
Ka	— Kapitza number defined in Eq. (4) (–)
L	— tube length (m)
L_v	— latent vaporization heat (J/kg)
\dot{m}	— mass flow-rate (kg/s)
Nu	— Nusselt number defined in Eq. (1) (–)
P	— pressure (mbar)
Pr	— Prandtl number defined in Eq. (3) (–)
Q	— overall heat flux (W)
Re	— Reynolds number defined in Eq. (2) (–)
R_g	— specific ideal gas constant (J/kg K)
r_d	— parameter defined in Eq. (7) (m)
r_i	— parameter defined in Eq. (8) (m)
r_t	— parameter defined in Eq. (9) (m)
SD	— standard deviation
T	— temperature (°C) and (K) in Eqs. (8)–(9)
U	— overall heat transfer coefficient (W/m ² K)
x	— constant in Eq. (17) (–)
y	— constant in Eq. (17) (–)

Greek symbols

ΔT	— temperature difference (K)
ΔP	— pressure difference (mbar)
$\Delta\sigma$	— surface free energy difference (N/m)
δ^+	— parameter defined in Table 1
γ	— heat capacity ratio (–)
Γ	— mass flow-rate per unit tube perimeter (kg/s m)
λ	— wall thermal conductivity (W/m K)
μ	— liquid dynamic viscosity (Pa s)
ν	— liquid kinematics viscosity (m ² /s)
θ	— contact angle (°)
ρ	— liquid density (kg/m ³)
ρ_v	— vapor density (kg/m ³)
σ	— surface tension, surface free energy (N/m)

Indices

cond	— condensation
CH ₂ l ₂	— diiodomethane
d	— dispersion
e	— external
exp	— experimental
evap	— evaporation

H ₂ O	— water
i	— inner
l	— liquid
lam	— laminar
mod	— model
p	— polar
s	— solid
swf	— salt water film
tur	— turbulent
w	— wall

References

- [1] P. Bandelier, J.J. d'Hurlaborde, F. Pelascini, M. Martins, A. Gonda, D. Alonso, M. Berlandisand F. Pigni. SOLMED: Solar energy and polymers for seawater desalination. *Desalin. Water Treat.* 55(12) (2015) 3285–3294.
- [2] P. Bandelier, J.J. d'Hurlaborde, F. Pelascini. MED seawater desalination using a low grade solar heat source, in: Presented in Conference on Desalination for Environment: Clean Water and Energy, EuroMed 2015, Palermo, Italy, May 10–14, 2015, *Desalin. Water Treat.* (in press).
- [3] E. Ghiazza, P. Peluffo. A new design approach to reduce water cost in MSF evaporators, IDA Conf., Bahamas, 2003.
- [4] J.B.P. Christmann, L.J. Krätz, H.J. Bart, Falling film evaporation with polymeric heat transfer surfaces, *Desalination* 308 (2013) 56–62.
- [5] T.B. Scheffler, A.J. Leao, Fabrication of polymer film heat transfer elements for energy efficient multi-effect distillation, *Desalination* 222 (2008) 696–710.
- [6] J.B.P. Christmann, L.J. Krätz, H.J. Bart, Novel polymer film heat exchangers for seawater desalination, *Desalin. Water Treat.* 21 (2010) 162–174.
- [7] J.B.P. Christmann, L.J. Krätz, H.J. Bart, PEEK film heat transfer surfaces for multi-effect distillation: A mechanical investigation, *Appl. Therm. Eng.* 38 (2012) 175–181.
- [8] A. Gonda, P. Lancereau, P. Bandelier, L. Luo, Y. Fan, S. Benezech, Water falling film evaporation on a corrugated plate, *Int. J. Therm. Sci.* 81 (2014) 29–37.
- [9] F. Kafi, V. Renaudin, D. Alonso, J.M. Hornut, New MED plate desalination process: Thermal performances, *Desalination* 166 (2004) 53–62.
- [10] K.R. Chun, R.A. Seban, Heat transfer to evaporating liquid films, *J. Heat Transfer* 93(4) (1971) 391–396.
- [11] A.A. Alhusseini, K. Tuzla, J.C. Chen, Falling film evaporation of single component liquids, *Int. J. Heat Mass Transfer* 41 (12) (1998) 1623–1632.
- [12] J. Han, L.S. Fletcher, Falling film evaporation and boiling in circumferential and axial grooves on horizontal tubes, *Ind. Eng. Chem. Process Des. Dev.* 24(3) (1985) 570–575.
- [13] R.W. Bonner, Correlation for dropwise condensation heat transfer: Water, organic fluids, and inclination, *Int. J. Heat Mass Transfer* 61 (2013) 245–253.
- [14] B.N. Taylor, C.E. Kuyatt, Guidelines for evaluating and expressing the uncertainty of NIST measurement results, Technical report, National Institute of Standards and Technology, Technical Note 1297 (1994) 24 pp.

- [15] A. Saul, W. Wagner, International equations for the saturation properties of ordinary water substance, *J. Phys. Chem. Ref. Data* 16 (4) (1987) 893–901.
- [16] W. Wagner, A. Pruss, International equations for the saturation properties of ordinary water substance. Revised according to the international temperature scale of 1990, *J. Phys. Chem. Ref. Data* 22(3) (1993) 783–787.
- [17] M.H. Sharqawy, J.H. Lienhard, S.M. Zubair, Thermophysical properties of seawater: A review of existing correlations and data, *Desalin. Water Treat.* 16 (2010) 354–380.
- [18] K.J. Bell, A.C. Mueller, *Heat Transfer Data Book II*, Wolverine Tube, Inc., 2001.
- [19] T. Roques-Carmes, H. Semara, C. Guyon, M. Tatoulian, S. Ognier, J.M. Commenge, Understanding of the liquid overflow behavior inside micro-structured falling film reactors based on a wetting approach, *Chem. Eng. Sci.* 118 (2014) 245–256.
- [20] T. Podgorski, J.M. Flesselles, L. Limat, Dry arches within flowing films, *Phys. Fluids* 11(4) (1999) 845–852.
- [21] T. Podgorski, Ruissellement en conditions de mouillage partiel (Runoff in partial wetting conditions). PhD thesis, Université de Paris 6, France, 2000.
- [22] J.W. Rose, Dropwise condensation theory and experiment: A review, *Proc. Inst. Mech. Eng. Part A: J. Power and Energy* 216(2) (2002) 115–128.
- [23] X. Ma, J.W. Rose, D. Xu, J. Lin, B. Wang, Advances in dropwise condensation heat transfer: Chinese research, *Chem. Eng. J.* 78 (2000) 87–93.
- [24] X.H. Ma, Dropwise condensation on PTFE coated surfaces and the catastrophe transition mechanisms between dropwise and film condensation. PhD thesis, Dalian University of Technology, China, 1994.
- [25] Q. Baojin, Z. Li, X. Hong, S. Yan, Heat transfer characteristics of titanium/water two-phase closed thermosyphon, *Energy Convers. Manage.* 50(9) (2009) 2174–2179.
- [26] D.K. Owens, R.C. Wendt, Estimation of the surface free energy of polymers, *J. Appl. Polym. Sci.* 13(8) (1969) 1741–1747.
- [27] F. Kafi, V. Renaudin, D. Alonso, J.M. Hornut, M. Weber, Experimental study of a three-effect plate evaporator: Seawater tests in La Spezia, *Desalination* 182 (2005) 175–186.
- [28] V. Renaudin, F. Kafi, D. Alonso, A. Andreoli, Performances of a three-effect plate desalination process, *Desalination* 182 (2005) 165–173.
- [29] H. Raach, J. Mitrovic, Seawater falling film evaporation on vertical plates with turbulence wires, *Desalination* 183 (2005) 307–316.
- [30] H. Raach, S. Somasundaram, J. Mitrovic, Optimisation of turbulence wire spacing in falling films performed with OpenFOAM, *Desalination* 267 (2011) 118–119.
- [31] W.M. Salvagnini, M.E.S. Taqueda, A falling-film evaporator with film promoters, *Ind. Eng. Chem. Res.* 43 (21) (2004) 6832–6835.